Combination Strategy for the Geocentric Realisation of Regional Epoch Reference Frames

A. Kehm[1], L. Sánchez[1], M. Bloßfeld[1], M. Seitz[1], H. Drewes[1], D. Angermann[1], F. Seitz[1]

[1]Deutsches Geodätisches Forschungsinstitut (DGFI-TUM), Technical University of Munich, Munich, Germany

Key Points:

- Geocentric datum realisation for regional epoch reference frames
- Combination of geodetic space techniques at normal equation level
- Long-term stability of the geocentric datum stability by a filtering approach

Corresponding author: Alexander Kehm, `alexander.kehm@tum.de`

Abstract

For high-resolution regional geodetic applications, the International Terrestrial Reference Frame (ITRF) is complemented by regional densifications. These are realised either as multi-year solutions related to a tectonic plate (e.g., EUREF for Europe) or as epoch reference frames (ERFs) to capture non-linear geophysical effects like earthquakes or loading displacements (e.g., SIRGAS for Latin America). These GNSS-only-based regional frames have in common that their geodetic datum is aligned with the ITRF datum at a specific epoch. Their origin is thus geocentric only in a mean sense and does not always coincide with the instantaneous centre of mass. Here, we present studies on a direct geocentric realisation of regional ERFs. We propose to realise the geodetic datum for each epoch by combining global GNSS, SLR and VLBI networks via measured local ties at co-located sites. An equally-distributed global GNSS network is used to realise the orientation via a no-net-rotation constraint and is densified by the stations of the regional subnetwork. The developed combination and filtering strategy aims to guarantee a stable datum realisation for each epoch-wise solution. The effectiveness of our methods is validated against the current operational realisation of the SIRGAS Latin American reference frame. Comparing with geophysical loading models relating to the Earth's centres of mass and figure, we show that the realised geocentric displacement time series directly reflect seasonal geophysical processes. Moreover, as the approach does not need to rely on co-location sites in the region of interest, it is conceptually transferrable to other global regions.

Plain Language Summary

In today's world, precise ground, sea and air navigation and the accurate monitoring of geophysical processes are vital. Precise coordinate reference frames make it possible to relate observed displacements to the Earth system. For different regions, these reference frames are materialised by dense networks of GNSS stations with precisely determined position coordinates. It is crucial that the origin (defined to coincide with the Earth's centre of mass), the scale (the realised unit of length) and the orientation (with respect to the Earth's body) of the reference frame match their conventional definition. The realisation of this so-called "geodetic datum" for current conventional reference frames suffers from several deficiencies. We have developed a strategy for the precise weekly geocentric realisation of regional reference frames. Coping with the changing and inhomogeneous distribution of stations observing different geodetic space techniques, we developed and implemented a strategy to improve the long-term stability of the solutions. We show that this approach allows for monitoring geophysical processes (loading and earthquakes) at low latency and overcomes the problems of existing realisations. The developed strategy is based on global networks and its effectiveness is proved in Latin America; however, it can be applied to any region of the Earth.

1 Introduction

Geodetic reference frames do not only provide the basis for surveying, mapping, or space-based positioning and navigation, but they are also the key fundament for the reliable localisation and quantification of changes in the Earth system (Plag & Pearlman, 2009). Continuous geodetic monitoring of the Earth's surface geometry, gravity field and orientation in space has enabled the precise determination of long-term and transient surface deformations and mass redistributions in the Earth's interior and its environment, including the oceans, atmosphere, hydrosphere and cryosphere. Measurements, data processing and estimated parameters must be related to a common and consistent reference frame to determine global change effects reliably. Presently, the International Terrestrial Reference Frame (ITRF, Altamimi et al., 2016; M. Seitz et al., 2016, 2021; Abbondanza

et al., 2017) is the global basis for the determination of coordinates on or near the Earth's surface and for the realisation of regional reference systems.

ITRF solutions are based on the combination of observation time series of four geodetic space techniques: Very Long Baseline Interferometry (VLBI), Satellite Laser Ranging (SLR), Global Navigation Satellite Systems (GNSS), and Doppler Orbitography and Radiopositioning Integrated by Satellite (DORIS). Each technique contributes to the realisation of the reference frame with particular strengths: the coordinate origin, which is defined to coincide with the centre of mass of the Earth system (CM) – i.e., solid Earth, oceans, hydrosphere, cryosphere and atmosphere –, is realised from SLR observations only. This is because SLR observations are most sensitive to the Earth's gravity field and less dependent on modelling uncertainties as they are inherent to GNSS and DORIS. The scale is realised from the weighted average of the VLBI and SLR scale information. GNSS and DORIS improve the station distribution worldwide. In addition, GNSS significantly contributes to the realisation of the orientation of the reference frame with respect to the Earth's surface due to the globally well-distributed station network. For recent ITRF solutions, the orientation is realised by the constraint of a no-net-rotation (NNR) to maintain the orientation of the new solution in accordance with its predecessor (Altamimi et al., 2016). According to the conventions of the International Earth Rotation and Reference Systems Service (IERS, Petit & Luzum, 2010), an ITRF solution is a set of mean station positions referring to a specific epoch and linear position changes over time (station velocities) that permit to infer coordinates at any time for all the stations considered in the computation. This linear parametrisation results in the origin of the ITRF reflecting the CM only in a mean sense (i.e., on secular time scales). For station displacements on seasonal and short time scales, the origin of networks aligned to the ITRF datum reflects the geometric centre of the Earth, often called the centre of figure (CF; Dong et al., 2003). As we focus on the interpretation of seasonal effects, hereafter we denote displacement time series that relate to an instantaneously realised CM as "CM-related" and displacement time series in a frame aligned to the ITRF datum as "CF-related".

Geophysical events (such as earthquakes) and instrumental updates induce changes in station positions or velocities. Consequently, it is necessary to recompute the ITRF coordinates regularly. Thus, ITRF solutions are released in intervals of several years, because the linearly extrapolated coordinates become too inaccurate for many applications and the ITRF loses its geocentricity after a few years. Recent ITRF releases also benefit from the increased accuracy of the contributions from the individual techniques as longer observation time series and improved background models are used in the data processing. The ITRF version currently in use is the ITRF2014 (Altamimi et al., 2016). Therein, linear station motions have been determined after applying a priori models for post-seismic trajectories approximated by logarithmic or exponential functions at stations affected by earthquakes.

Regional reference frames are necessary to ensure close-by accessibility to the global reference frame. In particular, GNSS users require reference stations near their areas of interest, while the ITRF station distribution is not dense enough for many applications. Therefore, regional reference frames are primarily realised as densifications of the ITRF through GNSS station networks, the technique used for most geodetic applications since it is cheaper and easier to handle than VLBI, SLR or DORIS. Regional reference frames are either realised as multi-year solutions related to a continental plate (e.g., the European Reference Frame EUREF/ETRS89; Altamimi, 2018) or as epoch reference frames (ERFs) to capture geophysical effects like earthquakes or loading displacements (e.g., the Sistema de Referencia Geodésico para las Américas SIRGAS; Sánchez et al., 2016). Their consistency with the ITRF is achieved by aligning the regional network via NNR, no-net-translation (NNT) or no-net-scale (NNS) constraints over either a regional or a global subset of common stations. The disadvantage of this alignment to linearly parametrised reference coordinates is that neither seasonal variations, for example caused by atmo-

spheric, oceanic and hydrological loading (F. Seitz & Krügel, 2009; F. Seitz et al., 2014; Glomsda et al., 2021a), nor episodic changes like seismic events (Sánchez & Drewes, 2016, 2020), nor anthropogenic changes such as subsidence due to groundwater withdrawal (e.g., Bevis et al., 2005), are fully modelled. The resulting coordinates are thus not strictly geocentric (neither in a mean sense nor instantaneously), and their information value for research of geodynamics or global change decreases substantially.

The two principal consequences of the usage of linearly modelled fiducial coordinates are:

(1) Mass variations in the atmosphere, the hydrology and the ocean lead to a relative variation between the CM and the CF (materialised by the stations of the reference frame), an effect often referred to as "geocentre motion" (e.g., Collilieux & Altamimi, 2009; Collilieux et al., 2009). Consequently, the reference frame is moving with respect to the (geophysical) geocentre (Drewes et al., 2013), meaning that the derived coordinates are inappropriate for a direct geophysical interpretation of environmental effects like loading-induced site displacements. The effects of this disagreement must be considered if the regional reference frame coordinates shall be assimilated into CM-frame-based geophysical models.
(2) Seismic events may cause considerable deformations, resulting in abrupt changes of point coordinates as well as changing station velocities in an extended area. As an example, Fig. 1 shows the station velocity changes at selected reference stations in Latin America induced by strong earthquakes since 2010. As the traditional multi-year reference frames provide station positions at a reference epoch and constant velocities derived from a limited data period, there is no reliable reference frame in these regions after earthquakes that occur in the extrapolation period of the reference frame (i.e., after the last observation epoch considered during its computation). By nature, this effect is inherent to all real-time applications. A geocentric reference frame should be computed at short time intervals to overcome this deficiency and to ensure a reliable basis for the operational activities based on GNSS positioning. This also holds for any other non-linear effects like monument motion, antenna deformation or anthropogenic changes that may result in continuously changing point coordinates that the linear velocity model cannot fully describe.

This study aims to develop a methodology to compute regional ERFs that are realised epoch-wise for short periods to cover non-linear station motions, that are geocentric at any epoch to relate these motions directly to geophysical phenomena, and that ensure a stable datum (origin, orientation, scale). We propose to realise the regional ERFs directly by combining GNSS with SLR and VLBI observations, omitting the usual alignment to a multi-year reference frame via fiducial points. Thereby, the origin and the scale are realised by SLR and VLBI while the orientation is realised by a non-deforming NNR constraint over a global GNSS network (Drewes, 2009). However, the datum parameters realised from SLR and VLBI suffer from an inhomogeneous station distribution and permanently changing observation network geometries. We thus propose to filter the SLR and VLBI information before the combination. The methodology shall be suitable to realise a series of ERFs with reliable geocentric station coordinates in near real-time at all epochs, especially after earthquakes. Furthermore, the resulting station coordinate time series shall be qualified to serve as a basis for the direct interpretation of station displacements in terms of geophysical processes.

We evaluate the developed methodology based on the Latin American network covered by SIRGAS. The SIRGAS network, located in one of the world's most seismically active regions, is affected by frequent strong earthquakes. In addition, an important number of stations are in the Amazon region, where seasonal variations in the time series may reach the decimetre level due to surface and ground water changes. Thus, Latin Amer-

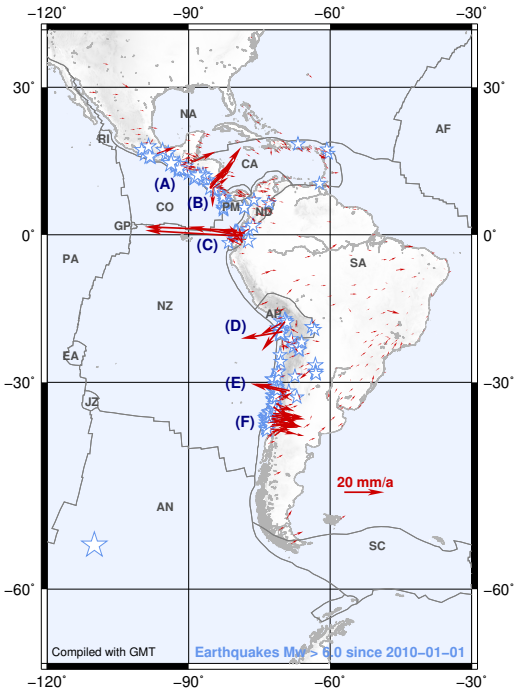

Figure 1. Changes in the Latin American reference frame kinematics induced by strong earthquakes. They are inferred from the difference between the two latest multi-year solutions SIR15P01 (Sánchez & Drewes, 2016) and SIR17P01 (Sánchez & Drewes, 2020). Stars represent earthquakes with Mw > 6.0 since Jan 1, 2010. The large discrepancies appear close to the epicentre of strong earthquakes: (A) Guatemala (Mw: 7.4, 2012-11-11), (B) Nicoya (Mw: 7.6, 2012-09-05), (C) Pedernales (Mw: 7.8, 2016-04-16), (D) Iquique (Mw: 8.2, 2014-04-01), (E) Illapel (Mw: 8.3, 2015-09-16), (F) El Maule (Mw: 8.8, 2010-02-27).

ica presents the ideal conditions to demonstrate the feasibility of a realisation of regional geocentric ERFs. Comparing the solutions with the ITRF as well as geophysical models of site displacements, we can clearly point out the benefits and deficiencies of our approach.

Within this study, we compute two solutions for geocentric weekly ERFs: an unfiltered (U-ERF) and a filtered ERF solution (F-ERF). The filter is applied at normal equation (NEQ) level to the SLR and VLBI networks before the inter-technique combination to reduce datum deficiencies related to station performances and varying network geometries. A reprocessed SIRGAS-like solution (SIRGAS-repro) aligned to the ITRF datum via fiducial points is used for validation. The two following sections outline our starting point based on the Latin American region (Sect. 2) and the general concepts on which our new approach is based (Sect. 3). Section 4 describes the input data and the pre-processing steps. The developed combination and filtering strategies are provided in Sect. 5. The results are discussed in Sect. 6; thereby, the F-ERF and the U-ERF solutions are compared to quantify the benefits from the filtering. A concluding summary and final discussions are provided in Sect. 7.

2 SIRGAS Reference Frame and Geodynamics in Latin America

SIRGAS is the regional densification of the ITRF in Latin America (SIRGAS, 1997; Drewes et al., 2005; Brunini et al., 2012; Sánchez et al., 2013, 2016). Currently, it is composed of about 400 continuously operating GNSS stations (Fig. 2, left panel). 70 of these stations are included in the IGS (International GNSS Service) global network (Johnston et al., 2017). The SIRGAS data-processing strategy follows the IERS conventions (Petit & Luzum, 2010) and the IGS's most-recent GNSS processing guidelines (Johnston et al., 2017). The only exception is that the GNSS satellite orbits and clock offsets as well as the Earth orientation parameters (EOPs) are not estimated within the SIRGAS processing but fixed to their weekly final IGS values (Johnston et al., 2017). Further details about the SIRGAS processing strategy are provided by Brunini et al. (2012); Sánchez et al. (2016); Sánchez and Drewes (2016).

The operational SIRGAS products are provided in weekly ERF solutions for station positions. The datum of a weekly operational SIRGAS solution (cf. Fig. 4, left column) is inherited from the respective IGS weekly solution via a 1 mm constraint over a regional subnet of common stations, the SIRGAS core stations (Sánchez & Kehm, 2021). The datum of the IGS weekly solution itself is aligned to the IGS reference frame via a global set of fiducial points that are extrapolated with linear coordinate changes, i.e., constant station velocities, from the reference epoch to the corresponding epoch (Rebischung et al., 2016).

An IGS reference frame is a selection of ITRF positions and velocities for a set of suitable GNSS stations, which are used as fiducial points for the generation of the IGS satellite orbits, satellite clock offsets and EOPs, as well as the corrections for the phase centre variations at both transmitting and receiving antennas. For instance, the IGS14/IGb14 reference frame (Rebischung & Schmid, 2016; Rebischung et al., 2016; Rebischung, 2020) corresponds to the ITRF2014 (Altamimi et al., 2016). As there is no translation, rotation, or scale difference between both reference frames (ITRF and IGS), the IGS final products and the computations based on them are considered in the corresponding ITRF datum (Kouba, 2009). Since the SIRGAS data analysis is based on the IGS reference frame valid when the GNSS data are routinely processed, the operational SIRGAS NEQs are given in different reference frames (details given in Sánchez & Kehm, 2021). Reprocessing campaigns of the historical data are regularly undertaken (Sánchez et al., 2016) to ensure consistency among the complete SIRGAS observation time series since 2000. A reprocessed series of solutions (here referred to as SIRGAS-repro) has been computed according to the most recent standards to avoid the impact of changes in the SIRGAS

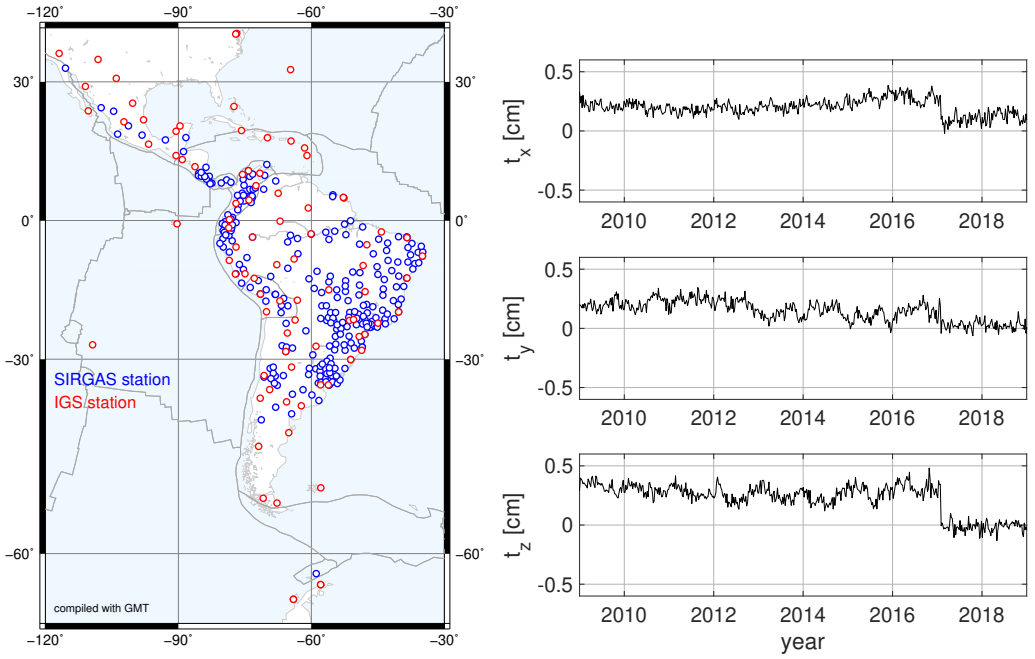

Figure 2. SIRGAS reference frame network (left) and translations of the SIRGAS/IGS weekly solution with respect to ITRF2014 (right). The translations have been determined via a 7-parameter similarity transformation of the global network of IGS core stations.

operational processing strategy and background models. It is constrained to the most recent series of IGS weekly solutions.

Due to the frequent occurrence of seismic events in the western margin of Latin America, the concept of conventional position/velocity solutions poses a practical problem. For instance, strong earthquakes result in global and regional reference frame solutions becoming inconsistent and the datum realisation via fiducial coordinates not being reliable any more. In addition to linear plate motion effects, time series of GNSS station positions show significant non-linear variations attributed to seismic events, post-seismic deformation or seasonal non-tidal loading (NT-L) effects (mainly in the vertical component), but they actually reflect a combined effect of non-modelled geophysical effects and uncertainties associated to the GNSS observations or GNSS data analysis (e.g., Blewitt et al., 2001; Collilieux et al., 2010, 2012; Drewes et al., 2013; Ray et al., 2008; Zou et al., 2014). These effects lead to a seasonal motion of the entire IGS weekly/SIRGAS network with respect to the ITRF origin (Fig. 2, right panel. The step visible in the translation time series is related to the switch of the applied PCV models for antenna phase centre variation from igs08.atx to igs14.atx in January 2017; see Rebischung et al., 2016). Therefore, one main challenge is to assess how much of the detected motion of a site is attributable to the uncertainties associated with the datum realisation and data processing, and how much is caused by mass variations or geophysical effects.

Fig. 3 displays the SIRGAS-repro time series of four stations located close to the Equator and to Antarctica, respectively. The two stations in far southern geographic latitudes (RIO2 and PALM) are affected by seasonal motions of similar amplitude in the North (N) component, albeit located on two different tectonic plates. In theory, one would expect these motions to be referrable to NT-L displacements in a CF-frame (as the SIRGAS datum is aligned to the linear ITRF origin). Projecting the translation time series of the SIRGAS-repro solution with respect to the ITRF origin into each station's local

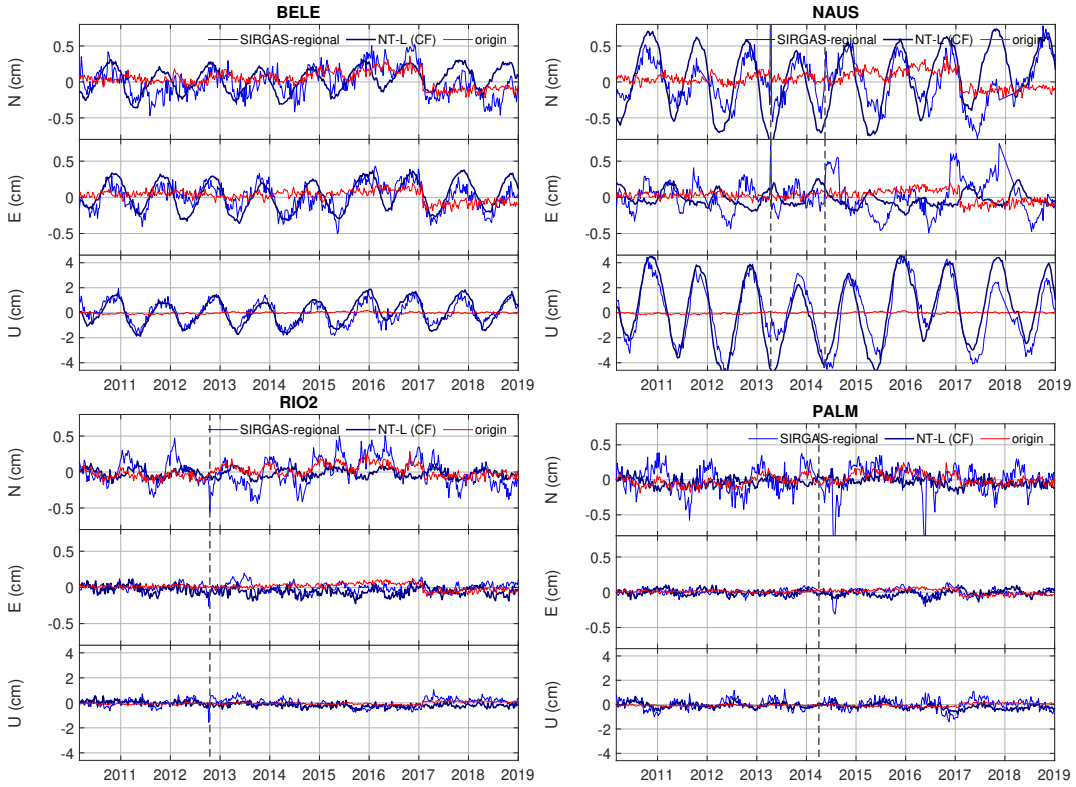

Figure 3. SIRGAS-repro coordinate time series of stations BELE (Belém, Brazil; top left), NAUS (Manaus, Brazil; top right) – both located in the Amazon basin –, RIO2 (Río Grande, Argentina; bottom left) located in Tierra del Fuego and PALM (Palmer) located in Antarctica compared to the ESMGFZ NT-L time series (Dill & Dobslaw, 2013) in CF-frame and to the variation of the SIRGAS origin with respect to the ITRF origin (Fig. 2, right panel, mapped into each station's local level system). A common disagreement with the NT-L time series is visible in the N component for Tierra del Fuego and Antarctica stations. This disagreement corresponds to the variation of the SIRGAS origin, which predominantly maps into the N component at high southern latitudes. Another common pattern is visible in the N and E components of the Amazon basin stations. Dashed vertical lines denote jumps removed from the position time series.

level system reveals that the deviation between modelled NT-L displacements and the site displacements observed is directly related to the variations in the origin. Similar common behaviour is visible for two stations in the Amazon basin (BELE and NAUS). In the equatorial region, the step induced by the switch in PCV models is mapped into the N and East (E) components. We can thus conclude that the SIRGAS origin, as currently realised, is not geocentric, neither in an instantaneous sense (CM-related) nor strictly in a mean sense (CF-related for seasonal changes). The first is expected as the datum is aligned to the multi-year linear ITRF datum, the second can be related to unmodelled fiducial point displacements or changes in background models that lead to a common motion of the whole reference frame. This common motion directly maps into the derived station position time series.

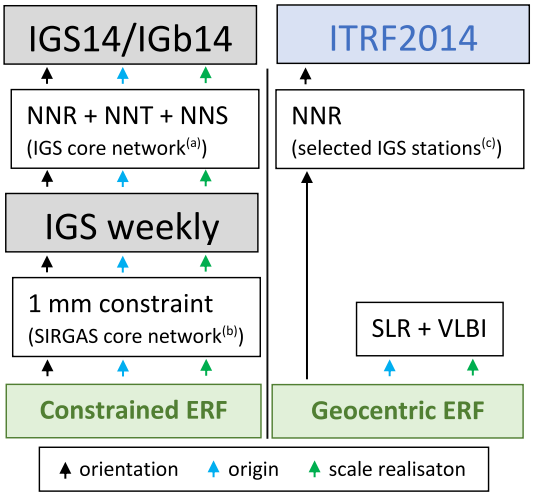

Figure 4. Concepts of datum realisation for the SIRGAS regional ERFs (left) and a direct geocentric realisation of ERFs (right). (a) cf. Rebischung et al. (2016); (b) cf. Sánchez and Kehm (2021); (c) cf. Sect. 4.1. The colours of the arrows refer to the different datum parameters. The datum of the IGS14/IGb14 and the ITRF2014 reference frames is considered identical.

3 Concept for a Direct Geocentric Realisation

Depending on the focus of interest, there are two possible ways of realising the datum of regional ERFs: The first would be to maintain the strategy as it is but improve the datum realisation via fiducial coordinates for a more accurate alignment with the ITRF datum. By these means, one could stick to the concept of processing GNSS-only-solutions, but consequently, coordinate variations would still be CF-related, i.e., the CM-minus-CF content of NT-L signals would still be missing in the station-specific displacement time series, as it is removed by the application of NNT constraints with respect to the ITRF. This would allow for a direct interpretation with respect to geophysics only after a correction of the CM-minus-CF variation from external geophysical models. Because of the growing interest in exploiting geodetic data for geophysical investigations, the second possibility would be a direct epoch-wise geocentric realisation of the datum of the ERFs, resulting in CM-related coordinates at each epoch. This would imply the processing not only of a globally-extended GNSS network but also of global SLR and VLBI networks. The great advantage of such a solution would be the direct interpretability of station displacement time series in a geophysical sense, without having to rely on external information on the motion of a multi-year reference frame with respect to the geocentre. By these means, geodetic observations could contribute directly to interpreting geophysical processes and the improvement and validation of geophysical models. Within this study, we investigate the second approach and have developed a strategy for a direct realisation of the datum of weekly regional geocentric ERF solutions based on the reference frame for Latin America.

Goal of this study are series of ERF solutions for Latin America, whereby the datum of each epoch-wise solution is defined consistently with the ITRS. The datum realisation is performed by combining the three geodetic space techniques of SLR, VLBI, and GNSS. The origin is realised by SLR – the only technique permitting its realisation with highest accuracy –, and the scale is realised as a weighted mean by SLR and VLBI. Because these two techniques are responsible for the physically defined datum parameters (in contrast to the orientation, which is defined by a mathematical constraint), we later denote these techniques as the “datum-relevant techniques”. The solution is com-

Table 1. Ratio of gaps ≥ 1 week in observation time series of VLBI and SLR stations between 2000 and 2014. Corresponding to our combination approach, the investigation is based on GPS weeks. In other words, a gap of one week means a full GPS week without a single observation.

gap length	SLR	VLBI
1 week	50.0 %	46.7 %
2 weeks	17.4 %	16.5 %
3 weeks	8.6 %	10.3 %
4 weeks	4.5 %	5.7 %
5–8 weeks	8.5 %	11.7 %
> 8 weeks	11.0 %	9.1 %

puted with minimum datum constraints to keep the geocentricity of the ERF. The orientation is realised via a NNR constraint over the global GNSS (IGS stations) network (Fig. 4). The datum transfer between the techniques is performed by introduction of local ties (LTs) at co-located sites, i.e., sites equipped with more than one of the geodetic space techniques used, and locally measuered difference vectors (ties) between the technique-specific reference points. Because, in our case, the target parameters are the positions of the GNSS stations contained in the regional network covered by SIRGAS, we do not include DORIS into the combination as this technique serves to densify the global ITRF station network (cf. Sect. 1) though it does not contribute to the datum parameters origin and scale.

One major issue in the realisation of ERFs is the so-called "network effect", i.e., apparent variations in the observed origin and scale caused by variations in the observing networks (e.g., Collilieux et al., 2009; Bloßfeld et al., 2014). Unfortunately, this effect is of special importance for the datum-relevant techniques SLR and VLBI, which both suffer from sparse and inhomogeneous network distributions. As demonstrated in various simulation studies (e.g., Pavlis & Kuźmicz-Cieślak, 2009; Otsubo et al., 2016; Glaser et al., 2017, 2019a, 2019b; Kehm et al., 2018, 2019), a substantial extension of the global SLR and VLBI networks would significantly stabilise the datum parameters realised.

However, for the time being, we must deal with the existing networks and their apparent variations due to the observational gaps of individual stations. Tab. 1 gives an overview of the gaps within the observation time series of VLBI and SLR stations. As can be seen, approximately 50 % of the gaps extend over one single week whereas about 10 % of the gaps extend over more than 8 weeks. Another approximately 10 % of the gaps have a length of between 4 and 8 weeks. To increase the stability of the networks, one major point of our study has thus been to investigate the way in which a filter approach allows sufficient bridging of these observational gaps to reduce the network effect, without systematically distorting the datum parameters realised (cf. Sect. 5.2).

4 Space Geodetic Input Data

4.1 Reprocessing SIRGAS Normal Equations for Combination with SLR and VLBI

An appropriate combination of global SLR, VLBI and GNSS networks is required to implement an epoch-wise datum realisation for regional networks. In our case, the regional GNSS network must be extended beyond the area covered by the SIRGAS network to include SLR/GNSS and VLBI/GNSS co-located stations and enough GNSS stations to realise the orientation via a NNR constraint. Therefore, one main objective of the study was to identify the GNSS network configuration required for a reliable datum realisation. Different scenarios were evaluated in this context. The first considered only

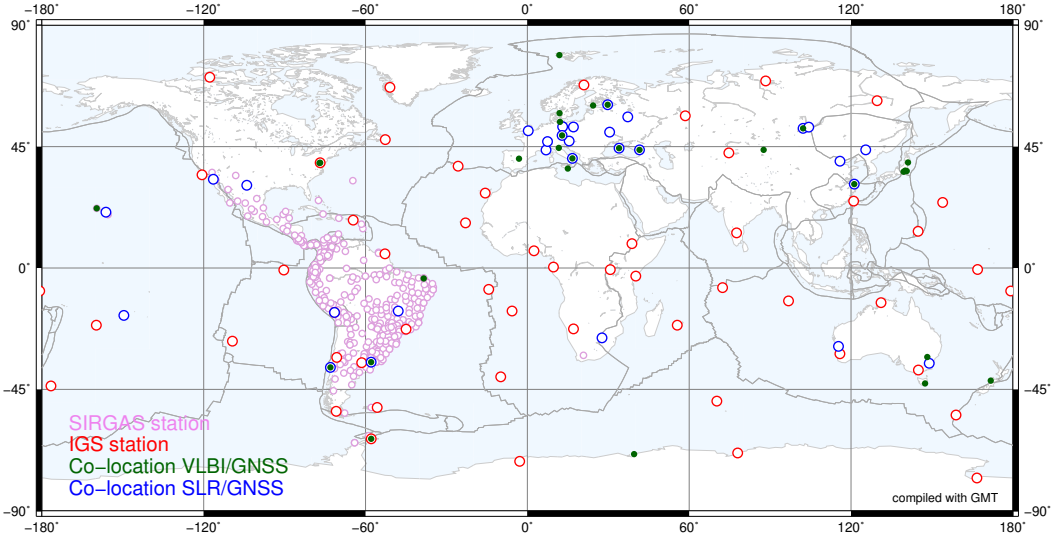

Figure 5. Extension of the SIRGAS network to enable its combination with VLBI and SLR as well as the realisation of the orientation via a NNR constraint.

those GNSS sites co-located with SLR and VLBI (blue circles and green dots in Fig. 5). As most of these stations are in the northern hemisphere, this station distribution did not turn out to be favourable for the GNSS data pre-processing. Consequently, additional GNSS sites have been included to ensure a more homogeneous global network distribution, which is also favourable for a reliable realisation of the orientation. After a series of empirical experiments, our main conclusion is to include the core stations of the IGS14/IGb14 reference frame into the GNSS data processing.

Further research concentrated on the simultaneous determination of GNSS satellite orbits, satellite clock offsets, EOPs and station positions within the GNSS data processing. Although we use a global network in the computations, simultaneous inclusion of all SIRGAS regional stations reduces the reliability of the EOPs and GNSS orbits due to the dense station distribution in one specific region (see Fig. 5). Therefore, we apply a two-step procedure: (a) orbit and EOP determination based on a global and homogeneous network, and (b) processing of the GNSS data (global + regionally densified network), whereby the previously determined orbits and EOPs are fixed. A priori datum information introduced into the GNSS NEQs by fixing the orbits and the EOPs is removed before combining them with the SLR and VLBI NEQs. This is performed by introducing and reducing (pre-eliminating) seven Helmert parameters (3 translations, 3 rotations and 1 scale parameter; cf. Bloßfeld, 2015). Thus, the GNSS NEQs introduced into the combination process are free from datum information.

The SIRGAS data reprocessing for this study covers January 2000 to December 2020. It is based on the IGS14/IGb14 reference frame and includes 530 SIRGAS and 135 IGS reference stations (30 co-located with SLR and 31 co-located with VLBI). This reprocessed global GNSS network is called the SIRGAS extended network hereafter. The GNSS data processing was carried out with the Bernese GNSS software Version 5.2 (Dach et al., 2015); the resulting weekly NEQs for combination are provided in the Solution INdependent EXchange Version 2.02 (SINEX v2.02) format (cf. IERS Message No. 103, 2006).

Table 2. Input data to the ERF combination.

technique	temporal resolution	processing setup *SINEX NEQ content*	datum constraints
SLR	weekly	future ILRS 5-satellite setup *station coordinates* *range biases* *EOPs*	no
VLBI	session-wise	CORE/NEOS/R1/R4 sessions *station coordinates* *source coordinates* *EOPs*	no
GNSS	weekly	SIRGAS + global IGS network *station coordinates*	yes (to be removed)

4.2 SLR and VLBI

Besides a full reprocessing of the SIRGAS GNSS network, the SLR and VLBI input data also underwent a full reprocessing to comply with the most recent standards and conventions (Petit & Luzum, 2010, including updates until v 1.3.0).

For SLR, we performed reprocessing specifically for this study. We extended the current standard four-satellite-constellation processed by DGFI-TUM in its function as an Analysis Centre (AC; Bloßfeld & Kehm, 2020) of the International Laser Ranging Service (ILRS; Pearlman et al., 2019), namely LAGEOS-1/2 (LAser GEOdynamics Satellite-1/2) and Etalon-1/2, by a fifth satellite, LARES (LAser RElativity Satellite). This is planned to be the future ILRS standard setup to ensure a higher stability of the SLR-derived origin (Bloßfeld et al., 2018). The satellites have been combined into weekly NEQs applying a variance component estimation (VCE) as described by Bloßfeld (2015). Satellite-specific parameters and orbits have been pre-reduced from the NEQs, leaving station positions and range biases as explicit parameters.

For VLBI, we rely on the VLBI contribution of DGFI-TUM to ITRF2020 (Glomsda et al., 2020). This dataset has no NT-L correction applied and is thus consistent with the routine processing standards of the other techniques. This contrasts with DGFI-TUM's routine contribution within its function as an AC to the International VLBI Service for Geodesy and Astrometry (IVS; Nothnagel et al., 2017), "dgf2020a", which contains a priori corrections for non-tidal atmospheric loading (Glomsda et al., 2021b). We use the twice-weekly CORE/NEOS (until 2001) and R1/R4 (from 2002 on) sessions, as these are available on a permanent twice-weekly basis and contain sufficient co-location sites for datum realisation. VLBI-specific parameters like troposphere and clock are pre-reduced and thus not explicitly contained in the NEQs. The properties of all technique-specific contributions are summarised in Tab. 2.

The SLR and VLBI NEQs are free from datum constraints and thus only contain the datum information to which the respective observations are sensitive. The SLR and VLBI data processing was carried out with the Orbit Computation (-OC) and Radio Interferometry (-RI) branches of the DGFI Orbit and Geodetic parameter estimation Software (DOGS; Gerstl, 1997; Bloßfeld, 2015), respectively. The resulting weekly (SLR) or session-wise (VLBI) NEQs for combination are provided in SINEX v2.02 format.

5 Combination Strategy

5.1 General Approach

This section is dedicated to describing the basic concept of the combination approach. The inter-technique combination is performed at the NEQ level (implementation at DGFI-TUM described in detail by Bloßfeld, 2015) with the DOGS-CS Combination and Solution library (Gerstl et al., 2000). Station positions are estimated within a least-squares adjustment according to the Gauß-Markov model (Gauss, 1823; Koch, 2004). Each NEQ system is set up by

$$\mathbf{N}\,\mathbf{d}\hat{\mathbf{x}} = \mathbf{y}, \tag{1}$$

consisting of the NEQ matrix $\mathbf{N}$, the vector of estimated parameters $\mathbf{d}\hat{\mathbf{x}}$ and the right-hand side of the equation system $\mathbf{y}$. The system is solved for $\mathbf{d}\hat{\mathbf{x}}$ by multiplication with the cofactor matrix of the estimated parameters

$$\mathbf{Q}_{\mathbf{d}\hat{\mathbf{x}}} = \mathbf{N}^{-1}, \tag{2}$$

and additionally yields the a posteriori variance factor

$$\hat{\sigma}_0^2 = \frac{\mathbf{v}^{\mathrm{T}}\mathbf{P}\mathbf{v}}{n-u}. \tag{3}$$

Here, $\mathbf{v}$ is the vector of observation residuals, n the number of observations and u the number of unknowns.

In the standard case of the Gauß-Markov model, $\hat{\sigma}_0^2$ serves to check whether the stochastic and functional models chosen a priori are consistent with the observations. If the latter is the case and if the a priori variance factor had been chosen as 1.0, then $\hat{\sigma}_0^2$ should also be close to 1.0. In this case:

$$\mathbf{Q}_{\mathbf{d}\hat{\mathbf{x}}} = \mathbf{\Sigma}_{\mathbf{d}\hat{\mathbf{x}}}, \tag{4}$$

with $\mathbf{\Sigma}_{\mathbf{d}\hat{\mathbf{x}}}$ being the variance-covariance matrix of the estimated parameters.

Weekly NEQs ($\mathbf{N}_{\mathrm{tech}}^{i}$) from SLR and GNSS and session-wise NEQs from VLBI are the input data for the combination. The processing for an epoch t_i comprises the following steps (Fig. 6):

(1.1) Pre-processing of the technique-specific NEQs. Calculation of intermediate single-technique (U-ST; "U" stands for "unfiltered") solutions.
(1.2) Rescaling of the technique-specific NEQs with their respective a posteriori variance factors from the U-ST solutions.
(2) Filtering the SLR and VLBI NEQs (F-ERF solution only). Calculation of intermediate filtered single-technique (F-ST) solutions.
(3.1) LT selection and weighting procedure based on the single-technique solutions.
(3.2) Inter-technique combination, the introduction of LT and NNR constraints and the subsequent solution of the combined NEQ.

In Step (1.1), incoming single-technique NEQs $\mathbf{N}_{\mathrm{tech}}^{i,\mathrm{ori}}$ are pre-processed for the combination. This includes accumulating the sessions of a week into one common NEQ for VLBI, reducing EOPs for SLR and VLBI, reducing range bias parameters for SLR, and eliminating source coordinates, i.e., fixing the celestial reference frame (CRF), for VLBI.

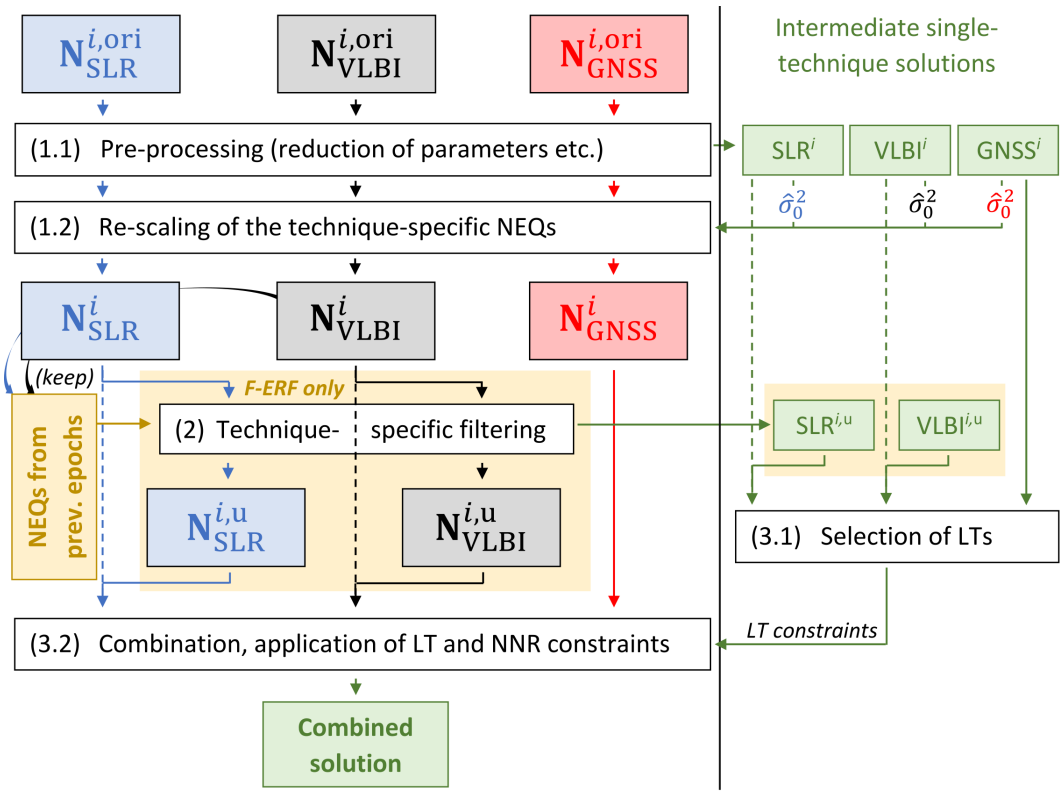

Figure 6. Concept of technique-specific filtering (SLR and VLBI) and inter-technique combination for epoch t_i. Dashed lines denote the unfiltered processing chain (U-ERF); light yellow boxes contain the additional steps performed only within the filtered processing chain (F-ERF).

The datum information from the GNSS NEQs is removed as described in Sect. 4. As a result, each NEQ is free from artificial datum information and only contains station coordinates as explicitly-estimated parameters. Afterwards, the intermediate U-ST solution is calculated with minimal constraints (i.e., NNR for SLR, NNR + NNT for VLBI, NNR + NNT + NNS for GNSS). The system is solved according to Eq. 1 and Eq. 2. The derived a posteriori variance factor $\hat{\sigma}_0^2$ (Eq. 3) is used to rescale the NEQ in Step (1.2). The U-ST solutions will be used for the LT selection and weighting procedure performed in Step (3.1). Moreover, they are used to validate the datum realisation (cf. Sect. 6).

Step (1.2) performs the rescaling of the NEQ with its reciprocal a posteriori variance factor $1/\hat{\sigma}_0^2$ to fulfil Eq. 4. The resulting pre-processed and rescaled technique-specific NEQ $\mathbf{N}^i_{\text{tech}}$ will be the actual input to the subsequent filtering and combination steps.

Step (2) performs the filtering for SLR and VLBI (F-ERF solution only): The single-technique NEQs are filtered before the combination (cf. Sect. 5.2) to guarantee an enhanced stability of the physically-derived datum parameters origin and scale. The outcome is a NEQ $\mathbf{N}^{i,\text{u}}_{\text{tech}}$ (where "u" stands for "updated") for this week, which is later used for the combination. Afterwards, the intermediate F-ST solution is calculated with minimal constraints. The SLR and VLBI F-ST solutions are introduced into the LT selection and weighting procedure performed in Step (3.1).

Step (3.1) performs the LT selection and weighting procedure (cf. Sect. 5.4). For the U-ERF solution, we use the GNSS solution and the U-ST solutions of SLR and VLBI from Step (1.1), while for the F-ERF solution, we use the GNSS solution from Step (1.1) and the F-ST solutions of SLR and VLBI from Step (2). The outcome is a set of LT constraint equations introduced into the combination and solution procedure performed in Step (3.2).

Step (3.2) performs the actual inter-technique combination. The technique-specific NEQs are combined into one NEQ

$$\mathbf{N}^i_{\text{comb}} = \lambda_{\text{SLR}} \cdot \mathbf{N}^{i,\text{u}}_{\text{SLR}} + \lambda_{\text{VLBI}} \cdot \mathbf{N}^{i,\text{u}}_{\text{VLBI}} + \lambda_{\text{GNSS}} \cdot \mathbf{N}^i_{\text{GNSS}}, \tag{5}$$

applying the technique-specific relative weights λ_{tech} (cf. Sect. 5.3). After introducing the LT constraint equations set up in Step (3.1) and adding a NNR constraint over a global selection of IGS stations (cf. Sect. 4.1), the solution is computed from the combined NEQ $\mathbf{N}^i_{\text{comb}}$ according to Eq. 1 and Eq. 2.

5.2 Filtering

All the pre-processing and combination steps are performed at the NEQ level. Consequently, we implement an information filter approach, a transfer of the Kalman filter (Kalman, 1960) approach from the solution level to the NEQ level (e.g., Chin, 2001; Assimakis et al., 2012). The approach thus enables us to apply relevant modifications directly to the NEQ systems without a need to solve the system beforehand. The filter generally implements a kinematic model that shall predict displacements of the stations within the network and a stochastic model that shall predict the evolution of their accuracy, or, in other words, the reliability of the predicted state.

As SLR and VLBI are the critical techniques for realising the physically-defined datum parameters for the regional GNSS network, their availability for each weekly ERF solution is crucial. Thereby, a network geometry that is as stable as possible must be achieved to minimise the network effect on the datum parameters realised. The developed filtering strategy needs to be a compromise between

(1) the optimal filling of observational gaps for single stations and
(2) the fact that the physical relevance of observations for the datum realisation is only given for a limited time span.

The information content to be derived from the NEQs of the datum-relevant techniques is uniquely related to their implicitly-contained datum information. This information is provided by the observing networks as a whole, and single stations at co-location sites serve to transfer the datum information to the GNSS network within the combined solution. Therefore, we are not interested in modelling motions of individual non-observing stations over long periods: The artificial information thereby introduced (based on assumptions) would potentially distort the realised datum. The contribution of a single station to the datum realisation shall be based solely on its observations. Consequently, the chosen kinematic filter model assumes positions of individual stations to be constant for a certain period without observations. Our filter's prediction step is thus intended to modify the stochastic information contained in the NEQ so that the decreasing reliability of the datum information due to unknown displacements is considered.

As a result of the considerations described above, we realise the prediction step by consistently modifying the complete stochastic information contained in the NEQ. Thereby, the prediction of a NEQ $\mathbf{N}_{\text{tech}}^{i-1}$ from epoch t_{i-1} to a NEQ $\mathbf{N}_{\text{tech}}^{i,\text{p}}$ at epoch t_i is performed by rescaling the NEQ with a factor κ:

$$\mathbf{N}_{\text{tech}}^{i,\text{p}} = \kappa \cdot \mathbf{N}_{\text{tech}}^{i-1} \tag{6}$$

Afterwards, the update step is performed, resulting in an updated NEQ

$$\mathbf{N}_{\text{tech}}^{i,\text{u}} = \begin{cases} \mathbf{N}_{\text{tech}}^{i,\text{p}} + \mathbf{N}_{\text{tech}}^{i} & \dots \text{if } \mathbf{N}_{\text{tech}}^{i} \text{exists,} \\ \mathbf{N}_{\text{tech}}^{i,\text{p}} & \dots \text{otherwise,} \end{cases} \tag{7}$$

with $\mathbf{N}_{\text{tech}}^{i}$ being the incoming information update for epoch t_i. Usually, an information update for SLR and VLBI is available every week (especially in our reprocessing scenario), so the second case is somewhat relevant for rare occasions of processing delays in the routine processing.

Because of the above requirement (2), we choose to filter the information from a specific epoch only over a limited period of w+1 weeks into the future (i.e., for all further prediction steps, the weighting factor κ is zero). Consequently, the filtered NEQ of epoch t_i is equal to a weighted sum of the NEQs from epoch t_{i-w} to epoch t_i. Each summand is only present if a NEQ for the respective epoch exists:

$$\mathbf{N}_{\text{tech}}^{i,\text{u}} = \sum_{n=0}^{w} \kappa^n \cdot \mathbf{N}_{\text{tech}}^{i-n} \tag{8}$$

The two filter parameters to be set are the filter weight κ to be applied within each prediction step and the "cut-off" number of prediction steps w after which the weight of a NEQ is set to zero.

For the determination of κ, auto-correlation functions have been computed for several stations that have observed continuously for multiple years and have not been affected by earthquakes. These functions follow a common pattern for both SLR and VLBI in all three coordinate components. This lets us compute an average auto-correlation function that roughly follows an exponential pattern for the first couple of weeks (Fig. 7). For both SLR and VLBI, the average auto-correlation $r(\Delta t)$ of the station position time

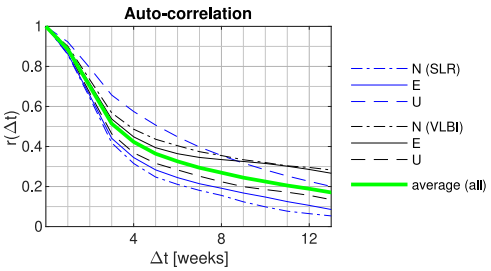

Figure 7. Average auto-correlation behaviour of selected SLR and VLBI site displacement time series.

series decreases weekly to about 0.5 after three weeks. From this, we deduce an approximate decrease factor of 0.8 per week. Introducing this into Eq. 6 as a rescaling factor $\kappa = 0.8$ means that the overall variance level of a NEQ is raised by a factor of $1/\kappa$ per prediction step, increasing the standard deviations for non-observing stations by about 12 %.

The cut-off number of prediction steps w has been chosen after three weeks (each prediction step is equivalent to a step of one week), meaning that a station will be present in the solution for no more than three weeks after its last observation. Concerning the above requirement (1), this yields approximately 75 % of the observational gaps within both the SLR and VLBI time series being bridged, leaving only the remaining 25 % of gaps that are longer than 3 weeks (cf. Sect. 3, Tab. 1). In this way, we significantly reduce the network effect (cf. Sect. 6.1). The cut-off prediction step yields a downweighting of the respective NEQ to a factor of $\kappa^3 = 0.51$ by applying the rescaling factor of $\kappa = 0.8$. The resulting standard deviations are scaled by a factor of 1.4 for stations that did not provide an observation update after this epoch.

5.3 Technique-Specific Weights

It is well known that the standard deviations of GNSS estimates are too optimistic due to neglected correlations (Schön & Kutterer, 2007; Schön & Brunner, 2008). This means that, although internally fulfilling the condition formulated in Eq. 4, the relative weight of the GNSS NEQ is too high compared to SLR and VLBI and could systematically distort the combined solution while simultaneously yielding too accurate standard deviations. Therefore, technique-specific a priori weights are determined by calculating the ratio between an empirically-derived weighted root mean square (WRMS) deviation and the average formal error (estimated standard deviation) of several representative and continuous coordinate time series. Thereby, the WRMS has been calculated from the time series content that can be considered noise rather than signal. The noise part of the time series has been extracted by applying a bandpass filter that sets the amplitudes of all periods above a threshold of 13 weeks (a quarter year) to zero, leaving only the short periods below the threshold. The coordinate time series have been chosen from stations that do not show significant peaks in the coordinate spectra for periods below the threshold. Table 3 gives the empirically-derived ratios between estimated standard deviations and the WRMS of the three-dimensional (3D) coordinate time series. The resulting ratio between WRMS and formal error is close to 1 for SLR and VLBI while it is close to 10 for GNSS. Consequently, the GNSS NEQs are introduced into the combination with an a priori scaling factor of $\lambda_{\mathrm{GNSS}} = 0.01$ while the scaling factor for SLR and VLBI is set up to $\lambda_{\mathrm{SLR}} = \lambda_{\mathrm{VLBI}} = 1.0$.

Table 3. Ratio between average estimated standard deviations and empirically-derived WRMS values (3D station coordinates; upper line) and technique-specific weights applied within the combination (lower line).

	SLR	VLBI	GNSS
$WRMS/\sigma$	1.3 ± 0.2	1.1 ± 0.3	9.7 ± 3.1
weight applied	1.0	1.0	0.01

Table 4. Average weekly number of LTs selected for the U-ERF and F-ERF solutions, resp., depending on the discrepancy criterion. The selected criterion is marked bold.

solution	discrepancy criterion	GNSS–SLR	GNSS–VLBI	SLR–VLBI	intra-tech.	total
U-ERF	30 mm	14.0	9.6	1.5	8.6	33.7
	50 mm	16.4	11.0	1.8	8.7	37.9
	70 mm	17.1	11.3	1.9	8.7	39.0
F-ERF	20 mm	14.0	11.5	2.2	7.4	35.1
	30 mm	18.1	13.9	2.8	8.7	43.5
	50 mm	20.3	15.6	3.0	8.8	47.7

5.4 Treatment of Local Ties

The datum transfer between the different techniques is performed by introducing measured LTs as constraints. Thereby, the global set of IGS GNSS sites included in the SIRGAS extended network ensures that all available co-locations between GNSS, SLR and VLBI can be exploited.

In this study, the LT treatment is based on the procedure described in detail by M. Seitz et al. (2012). The basis is the LT table initially compiled to realise the DTRF2014 (Bloßfeld et al., 2020). Concerning the techniques combined here, the table contains LTs for 95 inter-technique station pairs (49 GNSS–SLR pairs, 38 GNSS–VLBI pairs, 8 SLR–VLBI pairs) and 24 intra-technique station pairs (15 GNSS–GNSS pairs, 6 SLR–SLR pairs and 3 VLBI–VLBI pairs). Here, multiple measurements of the same LT are counted only once. The LT selection and weighting are performed independently for each epoch-wise ERF solution. The LT constraints are selected and weighted according to the discrepancy between the measured LT and the coordinate difference derived from the single-technique solutions. In the process, only LTs below a certain discrepancy threshold are considered. For the U-ERF solution, this threshold is chosen as 50 mm to achieve enough LTs per week (38 on average). A larger threshold of 70 mm would not yield a significant increase in the number of available LTs, but experiments showed that solutions might suffer from the introduction of single LTs which do not fit the local situation. This effect becomes worse when the threshold is further increased. For the F-ERF solution the threshold for LT introduction can be tightened to a discrepancy of 30 mm (cf. Tab. 4). Additional stations from the filtering enable the use of more LTs which fulfil a stricter discrepancy criterion. This yields a more stable datum realisation in the F-ERF solution than U-ERF solution (cf. Sect. 6.1).

To avoid systematic network deformations, some LTs must be excluded, especially at those stations affected by severe earthquakes (Tab. 5). This is necessary because LTs might still pass the selection procedure despite systematic errors. As a result, we consider it necessary to re-measure the LTs at affected stations after major seismic events.

Table 5. Sites co-located with GNSS with LTs excluded after major seismic events.

site	DOMES No.	technique	from	event
Concepción	41719M001	SLR	2010-02-27	Chile Earthquake
Concepción	41719S001	VLBI	2010-02-27	Chile Earthquake
Monument Peak	40497M001	SLR	2010-04-04	Baja Earthquake
Tsukuba	21730S007	VLBI	2011-03-11	Tōhoku Earthquake
Arequipa	42202M003	SLR	2017-07-18	Peru Earthquake

6 Results and Validation

6.1 Impact of Combination and Filtering on Datum Realisation

Tab. 6 summarises the impact of combination and filtering on the single-technique and combined solutions. Tab. 7 summarises the weighted mean and RMS deviations along the transformation time series of the U-ST and F-ST solutions of VLBI and SLR, respectively, with respect to ITRF2014; shown are the non-constrained datum parameters. Tab. 8 presents the weighted mean and RMS values along the transformation time series of the technique-specific subnetworks of the U-ERF and F-ERF solutions with respect to ITRF2014.

For the U-ERF solution, we can state that the datum realisation via the introduced LTs has no systematic effects on the datum-relevant technique-specific subnetworks. The comparison between the SLR U-ST solution and the combined U-ERF solution shows no significant impact on the SLR origin and scale; the same holds for the VLBI-derived scale (Tab. 6, U-ERF w.r.t. U-ST). The comparison of the solutions with respect to ITRF2014 (Fig. 8; Tab. 7, U-ST; Tab. 8, U-ERF) confirms that the transfer of the origin from SLR to the VLBI and GNSS networks is well-performed, although with a systematic effect of about $-3.5\,\mathrm{mm}$ in t_z for GNSS. A drift is observed in the scales of SLR and VLBI after 2015, the end of the observation period of the ITRF2014. The scale of the GNSS subnetwork lies between the scales from SLR and VLBI. This confirms that the combined scale is realised as a weighted mean of the SLR and VLBI scales.

For the F-ERF solution, we can state that filtering the datum-relevant techniques SLR and VLBI has no systematic effects on the realised datum parameters. The comparison between the U-ST and the F-ST solutions of SLR and VLBI shows no systematic impact on the subnetworks (Tab. 6, F-ST w.r.t. U-ST). The same holds for the combination step following filtering, which is seen by a comparison between the F-ERF and the F-ST solutions (Tab. 6, F-ERF w.r.t. F-ST). This confirms that the networks are not deformed by the selected LTs (all mean values are below $\pm 0.1\,\mathrm{mm}$ for the SLR origin and scale and $-0.04\,\mathrm{mm}$ for the VLBI scale).

While the general behaviour of both the F-ERF and the U-ERF solutions is identical (Fig. 8, Fig. 9), a significant decrease in the WRMS of the transformation parameters with respect to ITRF2014 is observed for the F-ERF solution compared to the U-ERF solution (Tab. 8). This is mostly due to a reduced noise of these time series which is caused by the increased network stability achieved in the F-ERF solution. A periodic variation is expected as each ERF solution is realised in an instantaneous CM-frame, whereas the ITRF2014 is a long-term CM-frame. It is important to note that the F-ERF solution also shows a reduction of the systematic offsets compared to the U-ERF solution, especially for t_z. For the GNSS network, the relative offset to the SLR origin is reduced to $-2.8\,\mathrm{mm}$. This can be related to the better distribution and a larger number of available LTs per week achieved by the filtering. The frequency spectra (Fig. 10) of the translations of the SLR solutions (U-ST and F-ST), the SLR subnetwork of the F-ERF solution and the GNSS subnetwork of the F-ERF solution agree in the main frequencies

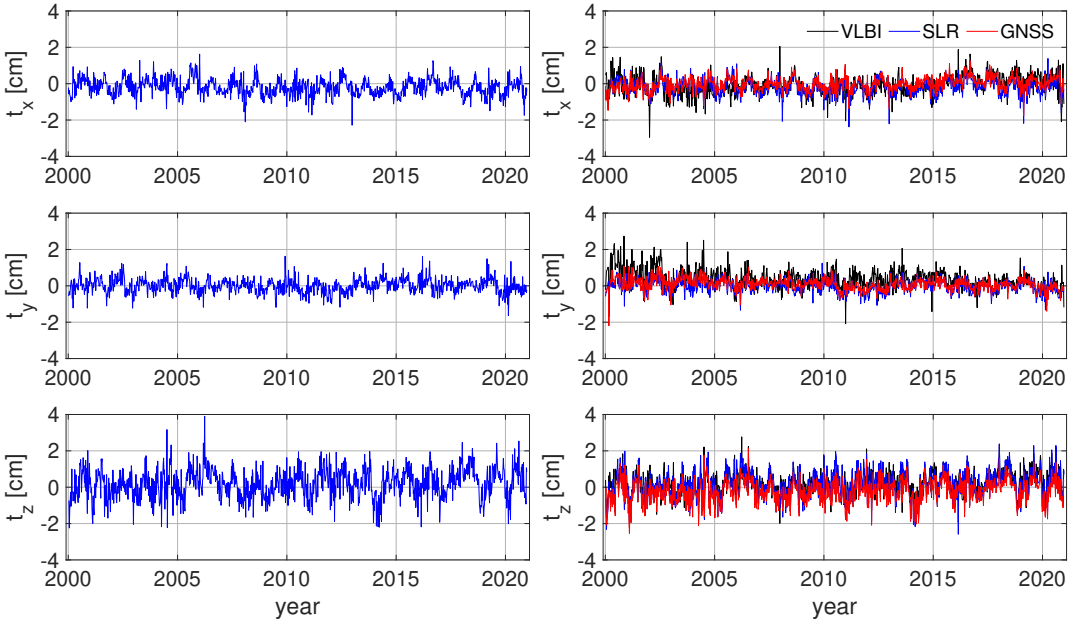

Figure 8. Translations with respect to ITRF2014 of the SLR single-technique solution (left) and the technique-specific subnetworks of the U-ERF solution (right).

Table 6. Impact of filtering and combination on the datum parameters derived by SLR and VLBI in terms of Helmert parameters between the solutions.

technique	datum parameter	U-ERF w.r.t. U-ST mean [mm]	U-ERF w.r.t. U-ST RMS [mm]	F-ST w.r.t. U-ST mean [mm]	F-ST w.r.t. U-ST RMS [mm]	F-ERF w.r.t. F-ST mean [mm]	F-ERF w.r.t. F-ST RMS [mm]
SLR	t_x	−0.1	0.6	0.3	2.4	0.0	0.3
	t_y	−0.1	0.5	−0.1	2.0	−0.1	0.3
	t_z	−0.4	1.2	−0.3	4.8	−0.3	0.5
	scale	0.2	0.5	−0.1	1.6	0.1	0.2
VLBI	*scale*	−1.1	2.2	0.0	2.9	−0.7	1.1

with a decrease in the yearly amplitude for GNSS. This damping may be related to the large and more homogeneously distributed global network (compared to SLR).

6.2 Interpretation of the Results with Respect to Geophysical Processes

In this section, we compare the F-ERF solution with loading models to quantify how well geophysical processes are represented in the time series. Our validation is based on geophysical fluid loading site displacement models (Dill & Dobslaw, 2013) provided by the Earth System Modelling group (ESMGFZ) of the Deutsches Geoforschungszentrum (GFZ) Potsdam. We use the sum of three NT-L components, namely non-tidal atmospheric (NTAL), non-tidal oceanic (NTOL) and hydrological loading (HYDL).

Fig. 11 shows the correlations between the displacement time series and the NT-L models in the CM-frame which are all positive. Fig. 12 shows the RMS differences between the site displacements and the NT-L models. For the N component, the RMS differences are generally higher than for the E component (0.40 cm as against 0.26 cm on average), especially in equatorial regions. This can mainly be related to the less stable

Table 7. Datum parameters of the single-technique solutions with respect to ITRF2014.

technique	datum parameter	U-ST Wmean [mm]	U-ST WRMS [mm]	F-ST Wmean [mm]	F-ST WRMS [mm]	Δ [%]
SLR	t_x	−1.6	4.4	−0.9	3.5	−20
	t_y	0.0	3.6	−0.4	2.8	−22
	t_z	2.2	7.7	1.6	5.7	−25
	scale	1.5	3.5	1.4	2.8	−18
VLBI	*scale*	4.8	4.6	4.7	3.1	−31

Table 8. Datum parameters of the combined solutions with respect to ITRF2014. In addition, Δ denotes the improvement of the WRMS of the F-ERF solution compared to the U-ERF solution.

technique	datum parameter	U-ERF Wmean [mm]	U-ERF WRMS [mm]	F-ERF Wmean [mm]	F-ERF WRMS [mm]	Δ [%]
SLR	t_x	−1.6	3.9	−1.1	3.3	−17
	t_y	−0.1	3.3	−0.4	2.7	−19
	t_z	1.5	7.1	1.2	5.4	−24
	scale	1.4	3.0	1.4	2.5	−18
VLBI	t_x	−0.6	4.5	−0.1	3.2	−29
	t_y	3.5	4.1	2.0	3.4	−17
	t_z	1.2	6.1	0.6	4.3	−30
	scale	3.4	3.6	3.5	2.9	−20
GNSS	t_x	0.0	3.5	0.6	2.7	−21
	t_y	0.9	3.1	0.7	2.3	−26
	t_z	−2.0	6.0	−1.7	4.3	−28
	scale	3.3	3.0	2.4	2.6	−15

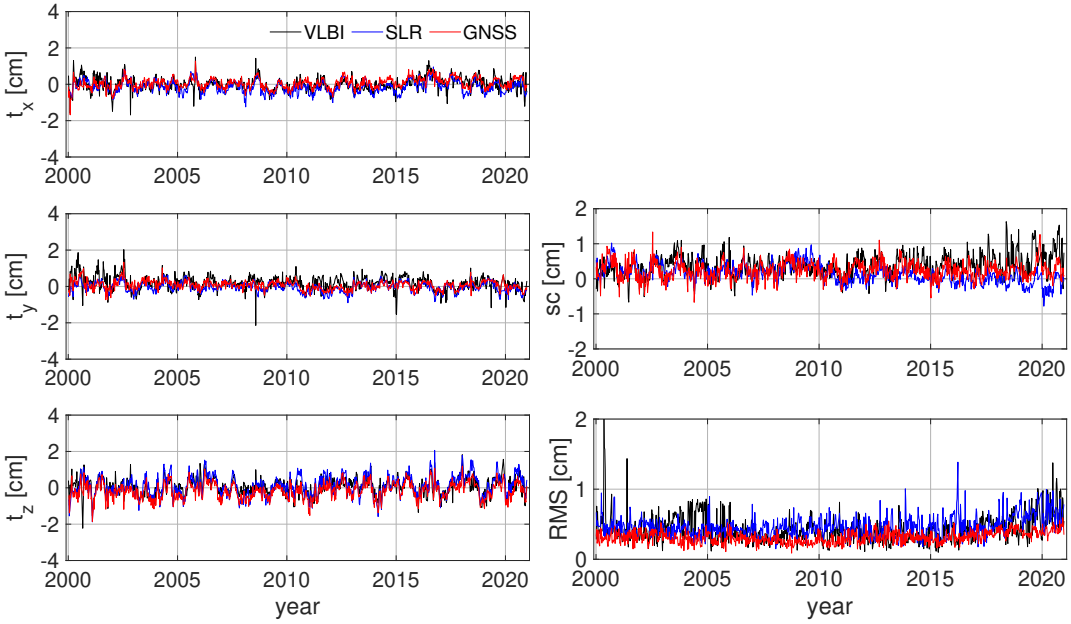

Figure 9. Translations (left), scale difference and RMS of the residuals of the Helmert transformation (right) of the F-ERF solution with respect to ITRF2014.

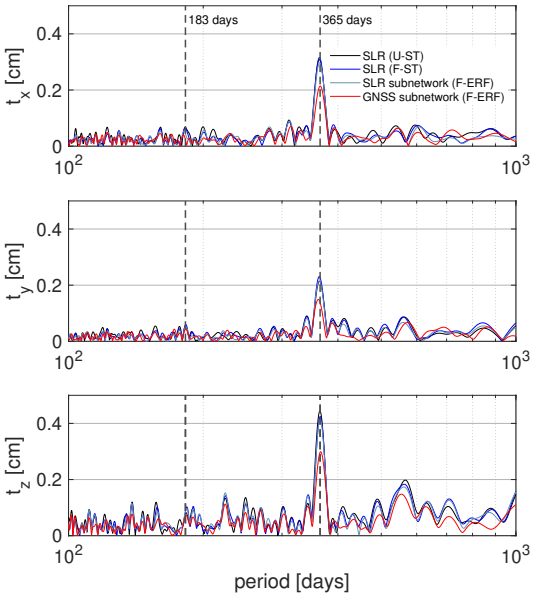

Figure 10. Spectra of the translation time series with respect to ITRF2014 of (1) the SLR U-ST solution, (2) the SLR F-ST solution, (3) the SLR subnetwork of the combined F-ERF solution and (4) the GNSS subnetwork of the combined F-ERF solution.

determination of the origin of the z-coordinate of the reference frame (cf. Fig. 9) and confirms a good agreement although the correlations for regions with a small effect are reduced due to the higher variations of the displacement and NT-L time series in the CM-frame. The largest RMS differences occur for the Up (U) component with an average of 0.62 cm and maximum values > 1 cm for time series in hydrologically active regions like the Amazon basin (such as for the NAUS site).

Fig. 13 shows the displacement time series for the sites discussed in Sect. 2. It is clearly visible that the F-ERF solution, in contrast to the SIRGAS-repro solution (cf. Fig. 3), closely follows the NT-L model relating to the CM-frame rather than that relating to the CF-frame. This confirms that the F-ERF solution reflects both local effects and the so-called geocentre variations and is thus suitable for a direct interpretation with respect to geophysical effects in a global context. However, for NAUS, a phase shift is visible in the E component between the NT-L time series provided by ESMGFZ and the observed site displacement time series, also when comparing the time series in a CF-related frame (Fig. 3). The effect might thus be related to model assumptions for the Earth's elastic deformation response in the hydrologically active Amazon basin (e.g., Martens et al., 2016).

7 Conclusions and Outlook

The paper presents series of weekly regional geocentric epoch reference frames (ERFs) for Latin America (SIRGAS network) with a direct datum realisation by combining global GNSS, SLR and VLBI networks. By implementing a filter method for the techniques SLR and VLBI, which are essential for the realisation of the origin and the scale, we could significantly improve the stability of the datum realisation. Compared to the unfiltered solution, the WRMS deviation, i.e., the scatter, of the realised epoch-wise origins of the regional GNSS network with respect to the ITRF origin could be reduced by 21 %, 26 % and 28 % in the x-, y- and z-components, respectively. This confirms the benefits of the

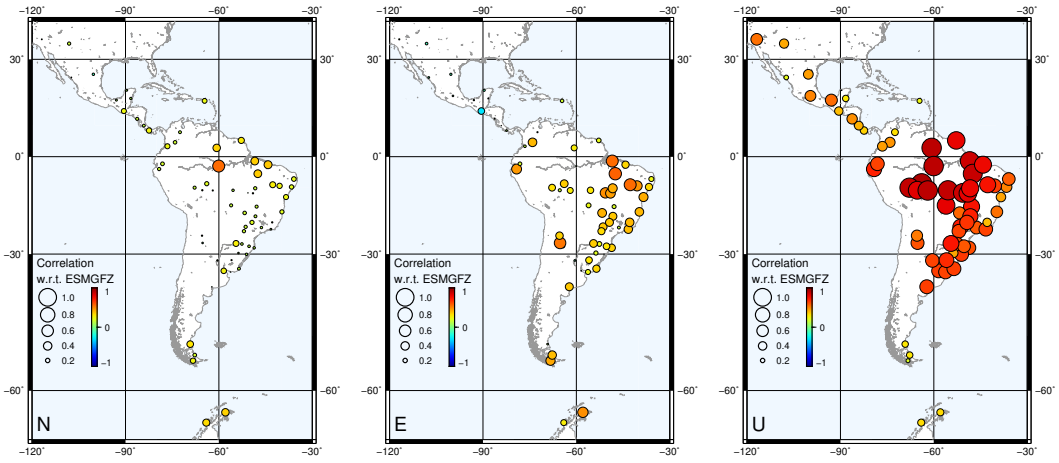

Figure 11. Correlations between the site displacement time series derived from the F-ERF solution and the ESMGFZ NT-L time series in CM-frame.

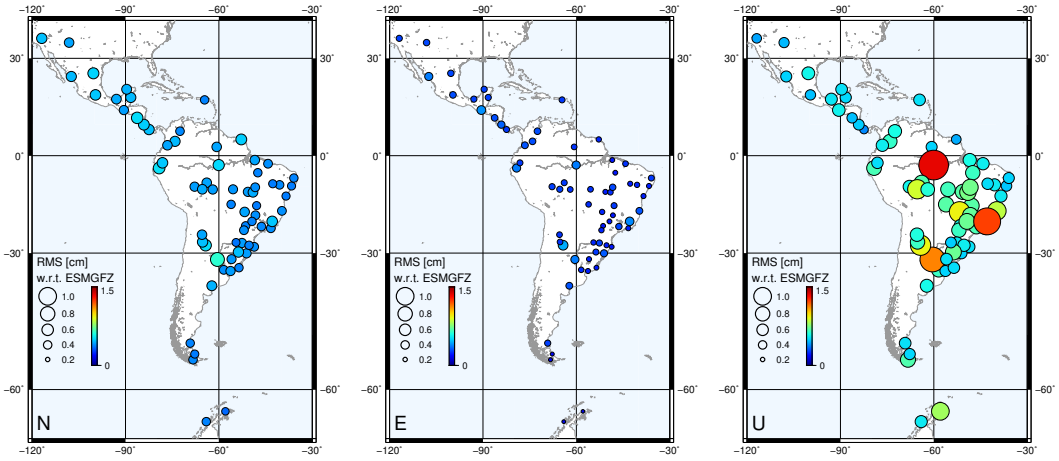

Figure 12. RMS difference between the site displacement time series derived from the F-ERF solution and the ESMGFZ NT-L time series in CM-frame.

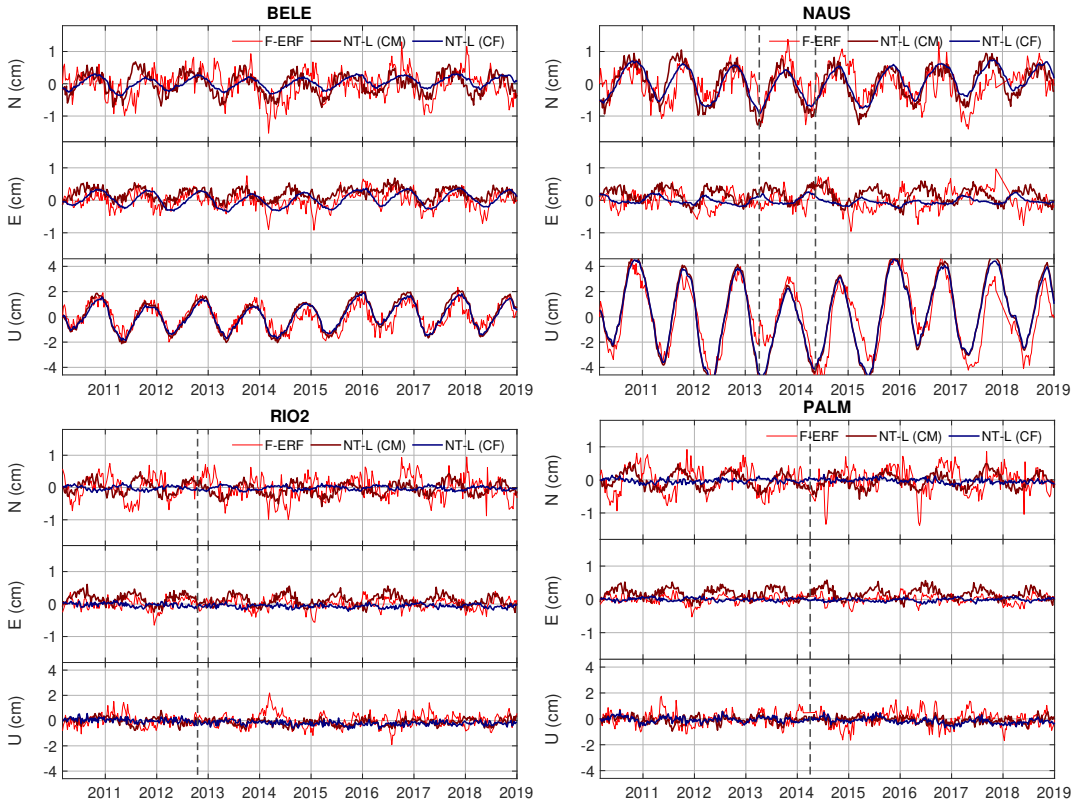

Figure 13. Coordinate time series of stations BELE, NAUS, RIO2 and PALM from the F-ERF solution compared with the ESMGFZ NT-L time series in CM- and CF-frame (cf. Fig. 3).

filtering approach and the importance of stable observational networks for realising geocentric ERFs.

Our approach is based on geodetic standard products currently available for VLBI and GNSS. In case of SLR, the ILRS 5-satellite setup extended by LARES has been used, which will become the routine ILRS-setup in the near future. As global networks serve to realise the datum, the combination strategy is not dominantly dependent on co-location sites (or, in the classical sense, fiducial stations) in the region of interest. As long as a sufficient number of globally well-distributed co-location sites with measured local ties (LTs) is available, the datum can be realised in a reliable way. Thus, the developed approach is conceptually transferable to any other region, independent of the number of locally available co-location sites.

The implemented combination methodology has demonstrated the capability of the filtering approach for bridging observational gaps particularly for the SLR and VLBI networks. Despite this, a further increase in station performances and availabilities, as recommended by various studies based on network and simulation analyses, will allow us to further improve the accuracy and temporal resolution of the ERFs. Especially the origin of the z-coordinate of the ERFs can potentially be improved in the near future by including more SLR satellites in highly-inclined orbits and additional SLR sites in near-polar regions in the solution. Another limiting factor for the datum transfer between the techniques is currently the non-standardised provision of LT measurements, which may lead to the problem of losing valid LT values in regions of high seismic activity. We consider it important that LTs be re-measured and published regularly so that all LT constellations are available with up-to-date values.

With the advantage of being geocentric at all epochs, the ERF solutions can improve the long-term reference, for example, to monitor the impacts of earthquakes, natural hazards and global change by means of GNSS. Thus, the fundamental benefit of the developed approach is that the resulting geodetic displacement time series can be directly used for studying the underlying geophysical processes. Furthermore, a common relation of various observation types from geodesy or geophysics to an instantaneously realised geocentre – the defined origin of the reference system – will enable their direct combination into one common system. The reference of all types of measurements to a common system realised geocentrically at any epoch will thus be a crucial contribution to achieving the ambitious goals of GGOS.

Acknowledgments

We gratefully acknowledge the partial funding of the research provided here by the German Research Foundation (DFG, grant no. SE 1916/5-1) within the framework of the project DIrect GEocentric Realisation of the American reference frame by combination of geodetic observation TechnIques (DIGERATI).

All data processed within this study is publicly available. SLR observation data is provided by the International Laser Ranging Service (ILRS) and has been accessed via the EUROLAS Data Centre hosted at DGFI-TUM (EDC, https://edc.dgfi.tum.de/en/; last access: 2021-08-11). VLBI observations are provided by the International VLBI Service for Geodesy and Astrometry (IVS) and has been accessed via NASA's Crustal Dynamics Data Information System (CDDIS, https://cddis.nasa.gov; last access: 2021-08-11). GNSS data of the global IGS stations is provided by the International GNSS Service (IGS) via NASA's CDDIS. The GNSS data of the SIRGAS stations has been provided by the SIRGAS Data Centres to DGFI-TUM as the IGS Regional Network Associate Analysis Centre for SIRGAS (www.sirgas.org).

References

Abbondanza, C., Chin, T. M., Gross, R. S., Heflin, M. B., Parker, J. W., Soja, B. S., ... Wu, X. (2017). JTRF2014, the JPL Kalman filter and smoother realization of the International Terrestrial Reference System. *Journal of Geophysical Research: Solid Earth*, *122*(10), 8474–8510. doi: 10.1002/2017JB014360

Altamimi, Z. (2018). *EUREF Technical Note 1: Relationship and Transformation between the International and the European Terrestrial Reference Systems* (Tech. Rep.). Retrieved from `http://etrs89.ensg.ign.fr/pub/EUREF-TN-1.pdf`

Altamimi, Z., Rebischung, P., Métivier, L., & Collilieux, X. (2016). ITRF2014: A new release of the International Terrestrial Reference Frame modeling nonlinear station motions. *Journal of Geophysical Research: Solid Earth*, *121*(8), 6109–6131. doi: 10.1002/2016JB013098

Assimakis, N., Adam, M., & Douladiris, A. (2012). Information filter and kalman filter comparison: Selection of the faster filter. In *Information Engineering* (Vol. 2, pp. 1–5).

Bevis, M., Alsdorf, D., Kendrick, E., Fortes, L. P., Forsberg, B., Smalley Jr, R., & Becker, J. (2005). Seasonal fluctuations in the mass of the Amazon River system and Earth's elastic response. *Geophysical research letters*, *32*(16). doi: 10.1029/2005GL023491

Blewitt, G., Lavallée, D., Clarke, P., & Nurutdinov, K. (2001). A new global mode of Earth deformation: Seasonal cycle detected. *Science*, *294*(5550), 2342–2345. doi: 10.1126/science.1065328

Bloßfeld, M. (2015). The key role of Satellite Laser Ranging towards the integrated estimation of geometry, rotation and gravitational field of the Earth. *Deutsche Geodätische Kommission (DGK) Reihe C*, *745*.

Bloßfeld, M., & Kehm, A. (2020). ILRS Analysis Activities. DGFI-TUM (Deutsches Geodtisches Forschungsinstitut Technische Universitt Mnchen), Germany. In C. Noll & M. Pearlman (Eds.), *International Laser Ranging Service 2016–2019 Report. NASA/TP-20205008530* (pp. 7-10–7-13). National Aeronautics and Space Administration, Goddard Space Flight Center, Greenbelt, MD, USA.

Bloßfeld, M., Rudenko, S., Kehm, A., Panafidina, N., Müller, H., Angermann, D., ... Seitz, M. (2018). Consistent estimation of geodetic parameters from SLR satellite constellation measurements. *Journal of Geodesy*, *92*(9), 1003–1021. doi: 10.1007/s00190-018-1166-7

Bloßfeld, M., Seitz, M., & Angermann, D. (2014). Non-linear station motions in epoch and multi-year reference frames. *Journal of Geodesy*, *88*(1), 45–63. doi: 10.1007/s00190-013-0668-6

Bloßfeld, M., Seitz, M., Angermann, D., & Seitz, F. (2020). DTRF2014: DGFI-TUM realization of the International Terrestrial Reference System (ITRS). In A. Z. & D. W. R. (Eds.), *IERS Technical Note 40* (pp. 5–16). Frankfurt am Main, Germany: Verlag des Bundesamtes für Kartographie und Geodäsie.

Brunini, C., Sánchez, L., Drewes, H., Costa, S., Mackern, V., Martínez, W., ... Da Silva, A. (2012). Improved analysis strategy and accessibility of the SIRGAS Reference Frame. In *Geodesy for Planet Earth. IAG Symposia 136* (pp. 3–10). Springer. doi: 10.1007/978-3-642-20338-1_1

Chin, T. (2001). On Kalman filter solution of space-time interpolation. *IEEE Transactions on Image Processing*, *10*(4), 663-666. doi: 10.1109/83.913601

Collilieux, X., & Altamimi, Z. (2009). Impact of the network effect on the origin and scale: case study of satellite laser ranging. In M. G. Sideris (Ed.), *Observing our Changing Earth. Proceedings of the 2007 IAG General Assembly, Perugia, Italy, July 2–13, 2007* (pp. 31–37). Springer.

Collilieux, X., Altamimi, Z., Coulot, D., van Dam, T., & Ray, J. (2010). Impact of loading effects on determination of the International Terrestrial Reference Frame. *Advances in space research*, *45*(1), 144–154. doi:

10.1016/j.asr.2009.08.024

Collilieux, X., Altamimi, Z., Ray, J., van Dam, T., & Wu, X. (2009). Effect of the satellite laser ranging network distribution on geocenter motion estimation. *Journal of Geophysical Research: Solid Earth*, *114*(B4). doi: 10.1029/2008JB005727

Collilieux, X., van Dam, T., Ray, J., Coulot, D., Métivier, L., & Altamimi, Z. (2012). Strategies to mitigate aliasing of loading signals while estimating GPS frame parameters. *Journal of Geodesy*, *86*(1), 1–14. doi: 10.1007/s00190-011-0487-6

Dach, R., Lutz, S., Walser, P., & Fridez, P. (Eds.). (2015). *Bernese GNSS Software Version 5.2* (Tech. Rep.). Berne, Switzerland: Astronomical Institute, University of Bern.

Dill, R., & Dobslaw, H. (2013). Numerical simulations of global-scale high-resolution hydrological crustal deformations. *Journal of Geophysical Research: Solid Earth*, *118*(9), 5008–5017. doi: 10.1002/jgrb.50353

Dong, D., Yunck, T., & Heflin, M. (2003). Origin of the International Terrestrial Reference Frame. *Journal of Geophysical Research: Solid Earth*, *108*(B4). doi: 10.1029/2002JB002035

Drewes, H. (2009). The actual plate kinematic and crustal deformation model APKIM2005 as basis for a non-rotationg ITRF. In H. Drewes (Ed.), *Geodetic Reference Frames. IAG Symposia 134* (pp. 95–99). Springer. doi: 10.1007/978-3-642-00860-3_15

Drewes, H., Angermann, D., & Seitz, M. (2013). Alternative definitions of the terrestrial reference system and its realization in reference frames. In *Reference frames for applications in geosciences* (pp. 39–44). Springer. doi: 10.1007/978-3-642-32998-2_7

Drewes, H., Kaniuth, K., Vö1ksen, C., Costa, S. M. A., & Fortes, L. P. S. (2005). Results of the SIRGAS campaign 2000 and coordinates variations with respect to the 1995 South American geocentric reference frame. In *A Window on the Future of Geodesy* (pp. 32–37). Springer. doi: 10.1007/3-540-27432-4_6

Gauss, C. F. (1823). Theoria combinationis observationum erroribus minimis obnoxiae. In *Commentationes Societatis Regiae Scientiarum Gottingensis recentiores Classis Physicae* (Vol. 5, pp. 33–90). Henricus Dieterich.

Gerstl, M. (1997). *Parameterschätzung in DOGS-OC. DGFI Interner Bericht MG/01/1996/DGFI, 2. Auflage* (Tech. Rep.). Munich, Germany: Deutsches Geodätisches Forschungsisnstitut.

Gerstl, M., Kelm, R., Müller, H., & Ehrnsperger, W. (2000). *DOGS-CS – Kombination und Lösung großer Gleichungssysteme. DGFI Interner Bericht MG/01/1995/DGFI* (Tech. Rep.). Munich, Germany: Deutsches Geodätisches Forschungsisnstitut.

Glaser, S., König, R., Ampatzidis, D., Nilsson, T., Heinkelmann, R., Flechtner, F., & Schuh, H. (2017). A Global Terrestrial Reference Frame from simulated VLBI and SLR data in view of GGOS. *Journal of Geodesy*, *91*(7), 723–733. doi: 10.1007/s00190-017-1021-2

Glaser, S., König, R., Neumayer, K. H., Balidakis, K., & Schuh, H. (2019b). Future SLR station networks in the framework of simulated multi-technique terrestrial reference frames. *Journal of Geodesy*, *93*(11), 2275–2291. doi: 10.1007/s00190-019-01256-8

Glaser, S., König, R., Neumayer, K. H., Nilsson, T., Heinkelmann, R., Flechtner, F., & Schuh, H. (2019a). On the impact of local ties on the datum realization of global terrestrial reference frames. *Journal of Geodesy*, *93*(5), 655–667. doi: 10.1007/s00190-018-1189-0

Glomsda, M., Bloßfeld, M., Seitz, M., & Seitz, F. (2021a). Correcting for site displacements at different levels of the Gauss-Markov model A case study for geodetic VLBI. *Advances in Space Research*, *68*(4), 1645–1662. doi:

https://doi.org/10.1016/j.asr.2021.04.006

Glomsda, M., Seitz, M., Angermann, D., & Gerstl, M. (2021b). DGFI-TUM Analysis Center Biennial Report 2019+2020. In D. Behrend, K. L. Armstrong, & K. D. Baver (Eds.), *International VLBI Service for Geodesy and Astrometry 2019+2020 Biennial Report. NASA/TP20210021389* (pp. 201–205). National Aeronautics and Space Administration, Goddard Space Flight Center, Greenbelt, MD, USA.

Glomsda, M., Seitz, M., Gerstl, M., Kehm, A., Bloßfeld, M., & Angermann, D. (2020). Impact of new models for the ITRF2020 in VLBI analysis at DGFI-TUM. In *AGU Fall Meeting 2020.* Retrieved from `https://mediatum.ub.tum.de/?id=1586328`

Johnston, G., Riddell, A., & Hausler, G. (2017). The international GNSS service. In P. J. G. Teunissen & O. Montenbruck (Eds.), *Springer handbook of global navigation satellite systems* (pp. 967–982). Springer. doi: 10.1007/978-3-319-42928-1

Kalman, R. E. (1960). A New Approach to Linear Filtering and Prediction Problems. *Transactions of the ASME–Journal of Basic Engineering*, *82*(Series D), 35–45.

Kehm, A., Bloßfeld, M., König, P., & Seitz, F. (2019). Future TRFs and GGOS–where to put the next SLR station? *Advances in Geosciences*, *50*, 17–25. doi: 10.5194/adgeo-50-17-2019

Kehm, A., Bloßfeld, M., Pavlis, E. C., & Seitz, F. (2018). Future global SLR network evolution and its impact on the terrestrial reference frame. *Journal of Geodesy*, *92*(6), 625–635. doi: 10.1007/s00190-017-1083-1

Koch, K.-R. (2004). *Parameterschätzung und Hypothesentests in linearen Modellen. Vierte, bearbeitete Auflage.* Ehemals Ferd. Dmmlers Verlag, Bonn. Retrieved from `http://www.geod.uni-bonn.de`

Kouba, J. (2009). *A guide to using International GNSS Service products.* Retrieved from `https://www.igs.org/wp-content/uploads/2019/08/UsingIGSProductsVer21_cor.pdf`

Martens, H. R., Simons, M., Owen, S., & Rivera, L. (2016). Observations of ocean tidal load response in South America from subdaily GPS positions. *Geophysical Journal International*, *205*(3), 1637-1664. doi: 10.1093/gji/ggw087

Nothnagel, A., Artz, T., Behrend, D., & Malkin, Z. (2017). International VLBI service for geodesy and astrometry – Delivering high-quality products and embarking on observations of the next generation. *Journal of Geodesy*, *91*(7), 711–721. doi: 10.1007/s00190-016-0950-5

Otsubo, T., Matsuo, K., Aoyama, Y., Yamamoto, K., Hobiger, T., Kubo-oka, T., & Sekido, M. (2016). Effective expansion of satellite laser ranging network to improve global geodetic parameters. *Earth, Planets and Space*, *68*(1), 1–7. doi: 10.1186/s40623-016-0447-8

Pavlis, E. C., & Kuźmicz-Cieślak, M. (2009). SLR and the next generation global geodetic networks. *Proceedings of the 16th International Workshop on Laser Ranging*. Retrieved from `https://cddis.nasa.gov/lw16/docs/papers/ggo_5_Pavlis_p.pdf`

Pearlman, M. R., Noll, C. E., Pavlis, E. C., Lemoine, F. G., Combrink, L., Degnan, J. J., ... Schreiber, U. (2019). The ILRS: approaching 20 years and planning for the future. *Journal of Geodesy*, *93*(11), 2161–2180. doi: 10.1007/s00190-019-01241-1

Petit, G., & Luzum, B. (2010). *IERS Conventions (2010). IERS Technical Note 36, v 1.3.0* (Tech. Rep.). Frankfurt am Main, Germany: International Earth Rotation and Reference Systems Service.

Plag, H.-P., & Pearlman, M. (Eds.). (2009). *Global Geodetic Observing System.* Springer.

Ray, J., Altamimi, Z., Collilieux, X., & van Dam, T. (2008). Anomalous harmonics

in the spectra of GPS position estimates. *GPS solutions*, *12*(1), 55–64. doi: 10.1007/s10291-007-0067-7

Rebischung, P. (2020). *Switch to IGb14 reference frame.* [IGSMAIL-7921]. Retrieved from `https://lists.igs.org/pipermail/igsmail/2020/007917.html`

Rebischung, P., & Schmid, R. (2016). *IGS14/igs14.atx: a new framework for the IGS products.* [AGU Fall Meeting 2016, abstract G41A-0998, San Francisco, CA, USA].

Rebischung, P., Schmid, R., & Herring, T. (2016). *Upcoming switch to IGS14/igs14.atx.* [IGSMAIL-7399]. Retrieved from `https://lists.igs.org/pipermail/igsmail/2016/001233.html`

Sánchez, L., & Drewes, H. (2016). Crustal deformation and surface kinematics after the 2010 earthquakes in Latin America. *Journal of Geodynamics*, *102*, 1–23. doi: 10.1016/j.jog.2016.06.005

Sánchez, L., & Drewes, H. (2020). Geodetic monitoring of the variable surface deformation in Latin America. In J. Freymueller & L. Sánchez (Eds.), *IAG Symposia 152.* doi: 10.1007/1345_2020_91

Sánchez, L., Drewes, H., Brunini, C., Mackern, M., & Martínez-Díaz, W. (2016). SIRGAS core network stability. In C. Rizos & P. Willis (Eds.), *IAG 150 Years. IAG Symposia 143* (pp. 183–191). Springer. doi: 10.1007/1345_2015_143

Sánchez, L., & Kehm, A. (2021). SIRGAS Regional Network Associate Analysis Centre (IGS RNAAC SIRGAS) Technical Report. In A. Villiger & R. Dach (Eds.), *International GNSS Service Technical Report 2020 (IGS Annual Report)* (pp. 135–146). IGS Central Bureau and University of Bern; Bern Open Publishing. doi: 10.48350/156425

Sánchez, L., Seemüller, W., Drewes, H., Mateo, L., González, G., Da Silva, A., ... Cimbaro, S. (2013). Long-term stability of the SIRGAS reference frame and episodic station movements caused by the seismic activity in the SIRGAS region. In Z. Altamimi & X. Collilieux (Eds.), *Reference Frames for Applications in Geosciences. IAG Symposia 138* (pp. 153–161). Springer. doi: 10.1007/978-3-642-32998-2_24

Schön, S., & Brunner, F. K. (2008). A proposal for modelling physical correlations of GPS phase observations. *Journal of Geodesy*, *82*(10), 601–612. doi: 10.1007/s00190-008-0211-3

Schön, S., & Kutterer, H. (2007). A comparative analysis of uncertainty modelling in GPS data analysis. In P. Tregoning & R. Rizos (Eds.), *Dynamic Planet: Monitoring and Understanding a Dynamic Planet with Geodetic and Oceanographic Tools. IAG Symposia 130* (pp. 137–142). doi: 10.1007/978-3-540-49350-1_22

Seitz, F., Hedman, K., Meyer, F. J., & Lee, H. (2014). Multi-sensor space observation of heavy flood and drought conditions in the Amazon region. In C. Rizos & P. Willis (Eds.), *Earth on the Edge: Science for a Sustainable Planet. IAG Symposia 139* (pp. 311–317). Springer. doi: 10.1007/978-3-642-37222-3_41

Seitz, F., & Krügel, M. (2009). Inverse model approach for vertical load deformations in consideration of crustal inhomogeneities. In H. Drewes (Ed.), *Geodetic Reference Frames. IAG Symposia 134* (pp. 23–29). Springer. doi: 10.1007/978-3-642-00860-3_4

Seitz, M., Angermann, D., Bloßfeld, M., Drewes, H., & Gerstl, M. (2012). The 2008 DGFI realization of the ITRS: DTRF2008. *Journal of Geodesy*, *86*(12), 1097–1123. doi: 10.1007/s00190-012-0567-2

Seitz, M., Bloßfeld, M., Angermann, D., Schmid, R., Gerstl, M., & Seitz, F. (2016). The new DGFI-TUM realization of the ITRS: DTRF2014 (data). *Deutsches Geodätisches Forschungsinstitut, Munich*. doi: 10.1594/PANGAEA.864046

Seitz, M., Bloßfeld, M., Angermann, D., & Seitz, F. (2021). DTRF2014: DGFI-TUM's ITRS realization 2014. *Journal of Advances in Space Research (submitted)*. doi: -

SIRGAS. (1997). *SIRGAS Final Report; Working Groups I and II IBGE, Rio de Janeiro* (Tech. Rep.). Retrieved from `http://www.sirgas.org/fileadmin/docs/SIRGAS95RepEng.pdf`

Zou, R., Freymueller, J. T., Ding, K., Yang, S., & Wang, Q. (2014). Evaluating seasonal loading models and their impact on global and regional reference frame alignment. *Journal of Geophysical Research: Solid Earth*, *119*(2), 1337–1358. doi: 10.1002/2013JB010186